Solid State Communications 253 (2017) 1–5

Contents lists available at ScienceDirect

Solid State Communications

journal homepage: www.elsevier.com/locate/ssc

Communication

# A DFT study of hypercoordinated copper silicide nanotubes

Ling-Yan Ai[a,b], Hui-Yan Zhao[a,c], Jing Wang[a,c], Ying Liu[a,c,*]

[a] Department of Physics and Hebei Advanced Thin Film Laboratory, Hebei Normal University, Shijiazhuang 050024, Hebei, China
[b] North China University of Science and Technology, Tangshan 063000, China
[c] National Key Laboratory for Materials Simulation and Design, Beijing 100083, China

ARTICLE INFO

*Keywords:*
Copper silicide nanotubes
Electronic structure
Density-functional theory calculations

ABSTRACT

The stability and electronic structures of copper silicide nanotubes (CuSiNTs) are calculated using first-principles density functional theory. Here these CuSiNTs of various different diameters, chiral vectors and morphologies were obtained by rolling up a novel two-dimensional hypercoordinated $Cu_2Si$ monolayer with high stability (Yang et al., J. Am. Chem. Soc. 137 (2015) 2757–2762). Electronic structure calculations showed that these CuSiNTs are conductors independent of their chiral vectors, diameters and morphologies. In addition, molecular dynamics (MD) simulations of the (6, 0) tube and the (8, 4) tube were performed. It was found that the (8, 4) tube has very good thermal stability and that its structure does not break down during MD simulations at initial temperatures up to 1500 K. Based on their electrical conductivity and good thermal stability, these CuSiNTs are promising candidates to envision application as metallic connections in nanoscale electronic devices.

## 1. Introduction

Silicon and carbon reside in the same group of the periodic table, and have the similar electronic configurations. Researchers have yet done a lot of studies to compare the electronic and structural properties of silicon with those of carbon. Since the carbon nanotubes (CNT) were first observed [1], there has been a considerable amount of researches, both experimental and theoretical, on silicon nanotubes (SiNTs).

Experimentally, a series of SiNTs have been synthesized in the laboratory using different techniques. In the early stage, it was reported that SiNTs were fabricated by the template process using substrate porous alumina [2,3], and using hydrogen-added dechlorination of $SiCl_4$ followed by chemical vapor deposition (CVD) on a $Ni_xMg_yO$ catalyst [4]. In the process of SiNTs formation, the disordered aggregation of silicon atoms was found inside the templates so good crystal structure cannot be formed. Later, the self-assembled growth of SiNTs by different methods was reported [5,6]. Then, there were several reports on the growth of SiNTs without solid templates. Such as, Xie *et al.* reported fabrication of SiNTs by a dual-RF-plasma treatment technique [7]. Silicon nanotubes (SiNTs) were synthesized from silicon monoxide using a hydrothermal method [8].

Theoretically, a large number of researches have been focused on the electronic, structural properties of SiNTs by diverse calculation approaches. Based on density functional theory, the electronic and structural properties of single-walled silicon nanotubes (SWSiNTs) were investigated. It is shown that their electronic properties are dependent of their chirality [9,10]. Then, armchair and zigzag SiNTs are discussed, with the results that armchair SiNTs are the most reasonable structures because of the efficient overlapping of *p* orbitals [11]. Barnard *et al.* [12] have also proved that the binding energy and strain energy of SWSiNTs depend on both their radius and chirality. In 2006, Yan *et al.* investigated single-crystalline silicon nanotubes (sc-SiNTs) [13] with $sp^3$ hybridization. Studies indicate that sc-SiNTs are energetically stable and the electronic property depends on the external diameter. Using density-functional tight-binding theory, Seifert *et al.* argued that the stability of silicate and SiH nanotubes are better than that of bare Si nanotubes [14]. Later, Guzmán-Verri *et al.* used a unifying tight-binding Hamiltonian when they investigated electronic properties of Si-based nanostructures. They found that SiNTs follow the so-called Hamada's rule [15].

Similarly, the stability of SiNTs by metal atoms [16–21] (Be, Zr, Sc, Ti, Cr, Fe, Ni and Co) placed along nanotubes axis have been investigated. Studies indicate that these atoms are essential for stabilizing the SiNTs. In addition, Durgun *et al.* [22] had studied (3, 3) SWSiNTs with transition metal (Ti and Cr) elements adsorbed on the external surface of SiNTs based on density-functional theory (DFT) calculations using ultrasoft pseudopotentials. They further found that such structures can be stabilized through doping by the transition metal Ti and Cr atoms.

Recently, Yang and co-workers predicted a novel and stable two-

* Corresponding author at: Department of Physics and Hebei Advanced Thin Film Laboratory, Hebei Normal University, Shijiazhuang 050024, Hebei, China.
*E-mail address:* yliu@hebtu.edu.cn (Y. Liu).

http://dx.doi.org/10.1016/j.ssc.2017.01.023
Received 9 May 2016; Received in revised form 10 December 2016; Accepted 23 January 2017
Available online 23 January 2017
0038-1098/ 

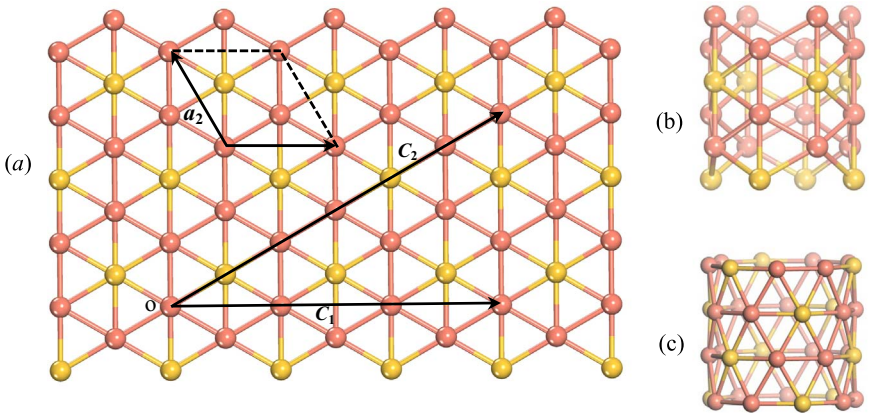


**Fig. 1.** (a) Geometric structure and lattice vectors ($\boldsymbol{a_1}$, $\boldsymbol{a_2}$) for the planar hexacoordinate $Cu_2Si$ monolayer. Two types of CuSiNTs can be rolled up with different chiral vectors of $\boldsymbol{C}_1$ and $\boldsymbol{C}_2$. The schematic representations, (b) (4, 0) CuSiNT, and (c) (6, 3) CuSiNT, of two ($m$, 0) and (2 $m$, $m$), respectively. Copper atoms are shown in salmon pink, and silicon atoms are dark yellow.

dimensional $Cu_2Si$ monolayer [23]. It reveals a perfect feature with planar hexacoordinate copper and planar hexacoordinate silicon. In the $Cu_2Si$ monolayer, however, each Cu connects with three Si atoms and three Cu atoms. Meanwhile, each Si atom is coordinated with six Cu atoms.

In this paper, we extend the work on $Cu_2Si$ monolayer to a discussion of CuSiNTs with various diameters and chiral vectors obtained by rolling up a $Cu_2Si$ monolayer, and carry out a comprehensive study of the stability and the electronic properties for the CuSiNTs using DFT calculations.

## 2. Calculation methods

Fig. 1 presents lattice vectors ($\boldsymbol{a_1}$ and $\boldsymbol{a_2}$), and chiral vectors ($\boldsymbol{C_1}$ and $\boldsymbol{C_2}$) of the planar hexacoordinate $Cu_2Si$ monolayer. The chirality of CuSiNTs is delineated by the chiral vector $\boldsymbol{C_i} = n_1\boldsymbol{a_1}+n_2\boldsymbol{a_2}$, where $n_1$, $n_2$ are integers. One CuSiNT with chirality can then be labeled with integer multiples of the lattice vectors, and denoted as ($n_1$, $n_2$). According to the chiral vectors ($\boldsymbol{C_1}$ and $\boldsymbol{C_2}$) shown in Fig. 1, there are two types of CuSiNTs, which are denoted as ($m$, 0) and (2 $m$, $m$), respectively. Here $m$ is interger. Fig. 1 present the (4, 0) CuSiNT, and (6, 3) CuSiNT as an example.

DFT calculations of the CuSiNTs were then performed in the generalized gradient approximations (GGA) [24]. The exchange-correlation potential was evaluated using Perdew, Burke and Ernzerhof (PBE) exchange-correlation functional [25], and a double-numerical basis set including polarization (DNP) was chosen for all atoms [26]. Core electrons were treated by semi-core pseudo potentials (DSPP) [27] for all atoms. The global orbital cutoff radius is set at 4.6 Å and the Monkhorst-pack scheme was used for k point sampling in the first irreducible Brillouin zone. All structures were allowed to relax using unrestricted spin and symmetry. During the geometry optimizations, the dispersion-correction approach of Tkatchenko and Scheffler (TS) scheme [28] was also used, and the convergence thresholds of the energy, the force and the atomic displacement were set to $10^{-5}$ Ha, 0.002 Ha/Å and 0.005 Å, respectively. During the self-consistent-field calculations, the convergence criteria were set to fine quality, with tolerance for the total energy of $10^{-6}$ Ha.

Ab-initio molecular dynamic (MD) simulations were carried out for a total time of 2 *ps* with a time step of 1.0 fs using microcanonical ensembles (NVE) in which the number of particles (N), volume (V) and temperature (T) remained constant. A 1×1×2 supercell was used for the (6, 0) tube and we adopted a supercell consisting of 1×1×3 repeated units for the (8, 4) tube. The diameters of the (6, 0) NT and the (8, 4) NT were 7.854 Å and 9.067 Å, respectively. MD simulations were carried out at initial temperatures of 600 K, 800 K, 1000 K and 1200 K for the (6, 0) NT and at initial temperatures of 600 K, 1200 K, 1500 K and 2000 K for the (8, 4) NT. The corresponding effective temperatures were 326.8 K, 432.7 K, 608.2 K and 733.6 K for the (6, 0) NT and 298.7 K, 582.8 K, 725.2 K and 1010.0 K for the (8, 4) NT.

## 3. Results and discussions

We first recalculated the structure of a two-dimensional $Cu_2Si$ monolayer using the above theoretical methods, with results as shown in Fig. 1. It may be seen that each Si atom connects to six Cu atoms in the same plane to form planar hexacoordinate motifs. Each Cu connects three Si atoms and three Cu atoms to form a hexacoordinate copper configuration in a two-dimensional plane. The optimized bond lengths for Si–Cu and Cu–Cu are 2.374 Å and 2.373 Å, respectively, which are close to the value of 2.38 Å obtained in previous calculations at the PAW/PBE level [23]. The computed binding energy of the $Cu_2Si$ monolayer was 3.584 eV/atom. Two Cu atoms and one Si atom are included in the unit cell of the $Cu_2Si$ monolayer.

We have performed a global search for the lowest-energy structures for these CuSiNTs with different diameters and chiral vectors. After structural relaxation and total-energy calculations for the CuSiNTs, stabilities and electronic properties of the ($m$, 0) and (2 $m$, $m$) NTs were calculated. The diameters of the ($m$, 0) NTs studied range from 4.225 to 13.089 Å and the diameters of the (2 $m$, $m$) NTs vary in the range 4.805–22.667 Å. To evaluate the stability of these CuSiNTs, the binding energy per atom is defined as $E_b = [2nE(Cu)+nE(Si)-nE(Cu_2Si)]/3n$, in which $E$(Cu) and $E$(Si) are the total energies of a single Cu and Si atom, the quantity $E(Cu_2Si)$ is the total energy of one $Cu_2Si$ unit cell. The binding energy per atom for the ($m$, 0) and (2 $m$, $m$) CuSiNTs versus the diameter is shown in Fig. 2. As can be seen from Fig. 2, for ($m$, 0) tubes, with increasing diameter, the binding energy per atom dramatically increases from 3.485 eV of (3, 0) tube to 3.574 eV of (10, 0) tube. In fact, the binding energy per atom for the CuSiNT (10, 0) is 3.574 eV/atom, very close to that of the $Cu_2Si$ monolayer, 3.584 eV. (See Table SI of the Supporting information). For (2 $m$, $m$) tubes, the increase in the binding energy per atom is similar to the trend for the ($m$, 0) NTs. With increasing diameter, their binding energies draw closer to that of the $Cu_2Si$ monolayer. In general, the CuSiNTs with large diameters have relatively high stability.

According to Fig. 2, the binding energy per atom of the (5, 0) NT is higher than that of the (6, 0) NT and the binding energy of the (8, 4) NT is higher than that of the (10, 5) NT. In order to investigate the greater stability of the (5, 0) and (8, 4) NTs, we have calculated the optimized average bond lengths of the CuSiNTs. From Fig. 1 we can see that there are Cu-Si bonds and Cu-Cu bonds for each type of nanotube. Fig. 3 illustrates how the average bond length changes with the diameter. For ($m$, 0) and (2 $m$, $m$) tubes, the average value of all bond lengths denoted by $L_1$ and $L_2$, decrease with the increasing tube diameter; from

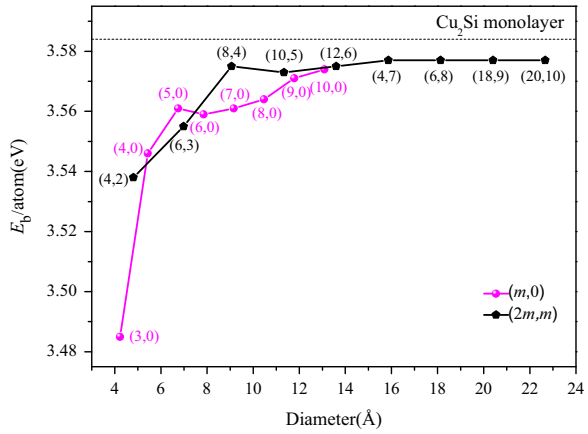


**Fig. 2.** Binding energy per atom for the CuSiNTs versus their diameters. See the text for nomenclature identifying the CuSiNTs.

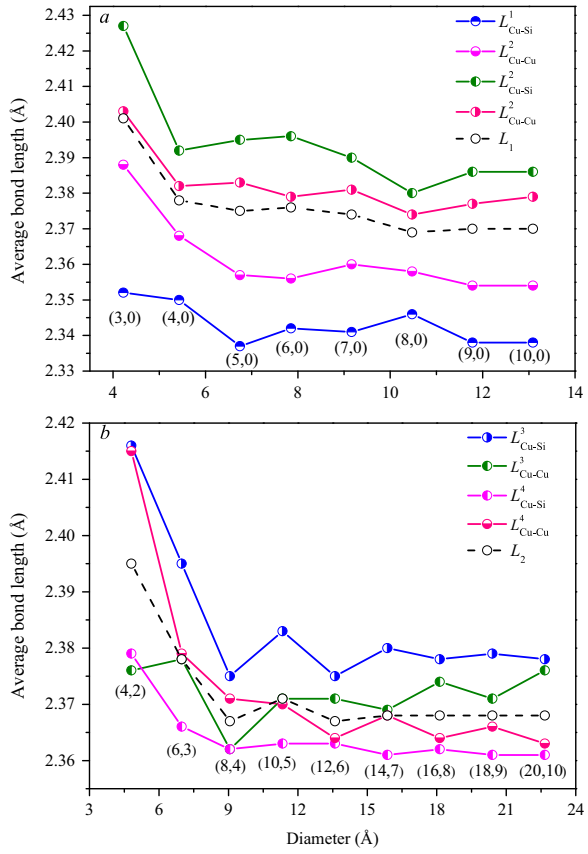


**Fig. 3.** Average bond lengths as a function of the diameter of the CuSiNTs; (a) Average bond length as a function of diameter for ($m$, 0) tubes. For the ($m$, 0) NTs, the bonds parallel to the tube axis are Cu-Si bonds and Cu-Cu bonds, average bond lengths are labeled $L^1_{Cu-Si}$ and $L^1_{Cu-Cu}$. The average bond lengths of other bond types for the Cu-Si bond and Cu-Cu bond are labeled $L^2_{Cu-Si}$ and $L^2_{Cu-Cu}$, respectively. (b) Average bond length as a function of diameter for (2 $m$, $m$) tubes. For the (2 $m$, $m$) tubes, the average bond lengths of perpendicular to the tube axis Cu-Si bonds and Cu-Cu bonds are labeled $L^3_{Cu-Si}$ and $L^3_{Cu-Cu}$, respectively. The others types of Cu-Si and Cu-Cu bonds are labeled $L^4_{Cu-Si}$ and $L^4_{Cu-Cu}$. For ($m$, 0) and (2 $m$, $m$) tubes, the average value of all bond lengths denoted by $L_1$ and $L_2$.

the Fig. 3a, it may be seen that the average bond lengths $L_1$ of the (5, 0) NT are shorter than for the (6, 0) NT. The average bond lengths of the (5, 0) NT are dominated by the average Cu-Si and Cu-Cu bond lengths which are parallel to the tube axis (see Fig. 3a). On the other hand, as may be seen in Fig. 4, the deformation charge density of the (5, 0) NT shows charge transfer from each Cu atom to each Si atom. Hirshfeld charge analysis indicates a charge transfer of 0.056 e from each Cu atom in which Cu 4 s electrons are transferred and are delocalized around the three Cu-Si bonds and three Cu-Cu bonds. At the same time, electrons from the 3p state of the Si atoms are also found to be partially depleted and delocalized over the six Cu-Si bonds. The Cu-Si bonds along the tube axis accumulate more charges than Cu-Si bonds lying in other directions and the Cu-Cu bonds along the tube axis gather more charges than Cu-Cu bonds lying in other directions.

For the (8, 4) tube, the major contribution to the average bond lengths $L_2$ comes from the Cu-Si and Cu-Cu bonds that are perpendicular to the tube axis. The average Cu-Si and Cu-Cu bond lengths perpendicular to the tube axis are shorter than those of the (10, 5) NT (see Fig. 3c).

The final structures in each MD simulation are shown in Fig. 5 in both a side view and top view. For the (6, 0) tube, it can be seen that its structure can maintain its structural integrity at effective temperatures up to 432.7 K. During simulations with effective temperatures of 608.2 K, the system starts to disrupt. For the (8, 4) tube, its structure does not disrupt up to an effective temperature of 725.2 K showing that the (8, 4) tube has high thermal stability. The system is seriously disrupted when the effective temperature is 1010.0 K.

To investigate the electronic properties, we calculated the electronic band structures and the corresponding projected density of states (PDOS) of the CuSiNTs. Selected results are shown in Figs. 6 and 7 while full data are given in the Fig. S1 of Supporting Information. It was found that all the CuSiNTs rolled from the two-dimensional $Cu_2Si$ monolayer in our calculations exhibited metallic conductivity with the bands crossing the Fermi level without a band gap at this energy level. Below the Fermi level there are more Cu-3d states than other electron states. At the Fermi level, it indicates that there is hybridization between the Si-3p, Cu-3d and Cu-4p states.

Fig. 7 illustrates selected typical geometric configurations and the corresponding band structure and DOS for the (6, 0) and (8, 0) NTs. Note that for the (8, 0) NT, several bands are close to the Fermi level, which ensures a significant carrier density. The bands are degenerate at the Γ-point and they are dispersive along the $\Gamma$-$X$ axis, which implies a smaller effective mass for the charge carriers [29,30]. Smaller effective mass of the charge carriers implies high mobility and high conductivity. Hence, the CuSiNTs could have potential applications as metallic connections in electronic devices.

## 4. Conclusions

In summary, using DFT, we have investigated a series of CuSiNTs with various diameters, chiral vectors and morphologies on the basis of the hexacoordinate $Cu_2Si$ monolayer. The results show that the ($m$, 0) [$m$=3–10] and (2 $m$, $m$) [$m$=2–10] nanotubes are metallic independent of their chiral vectors, diameters and morphologies. Within the scope of our research, except for the (6, 0) tube, all the CuSiNTs are nonmagnetic metals. The MD simulations of the (8, 4) tube shows that it has very good thermal stability and can maintain its structural integrity up to an effective temperature of 725.2 K. Given their electrical conductivity and good thermal stability these CuSiNTs may find application as metallic connections in nanoscale electronic devices.

## Acknowledgements

The authors thank Dr. N. E. Davison for his help with the language. This work is supported by the National Natural Science Foundation of China (Grant Nos. 11274089, U1331116, 11304076, and 11547198), the Natural Science Foundation of Hebei Province (Grant No. A2015205179), and the Science Foundation of Hebei Education department for Distinguished Young Scholar (Grant No. YQ2013008), and the Program for High-level Talents of Hebei Province (Grant No. A201500118). We also acknowledge partially financial support from the 973 Project in China under Grant No. 2011CB606401.

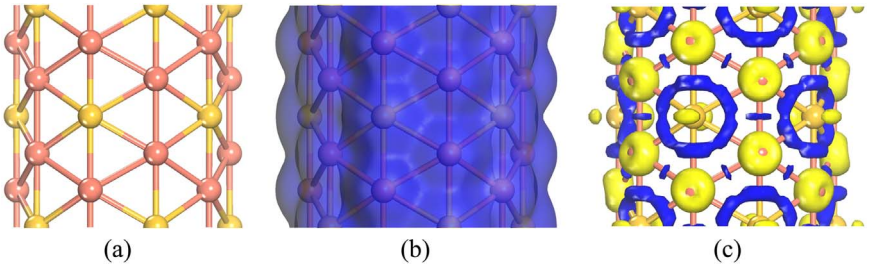


**Fig. 4.** (a) A ball and stick model for the (5, 0) NT from a perspective perpendicular to the tube axis. (b) Isosurface plots (0.2 e/Å3) of the total charge density for the (5, 0) NT. (c) Isosurface plots (0.062 e/Å3) for the deformation charge density of the (5, 0) NT. Charge accumulation and depletion regions are in blue and yellow, respectively. Copper atoms are red, and silicon atoms are dark yellow.

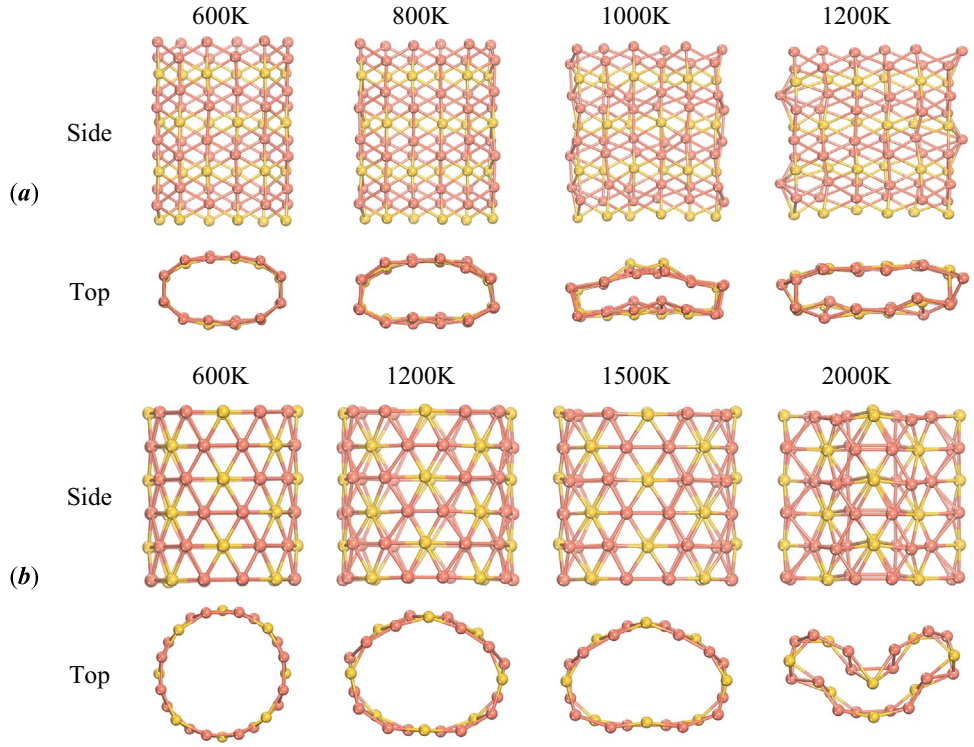


**Fig. 5.** The final frames of the molecular dynamics simulations for the (6, 0) NT (*a*) and the (8, 4) NT (*b*) at different initial temperatures. Side views (Side) perpendicular to the tube axis and top views (Top) along with the tube axis.

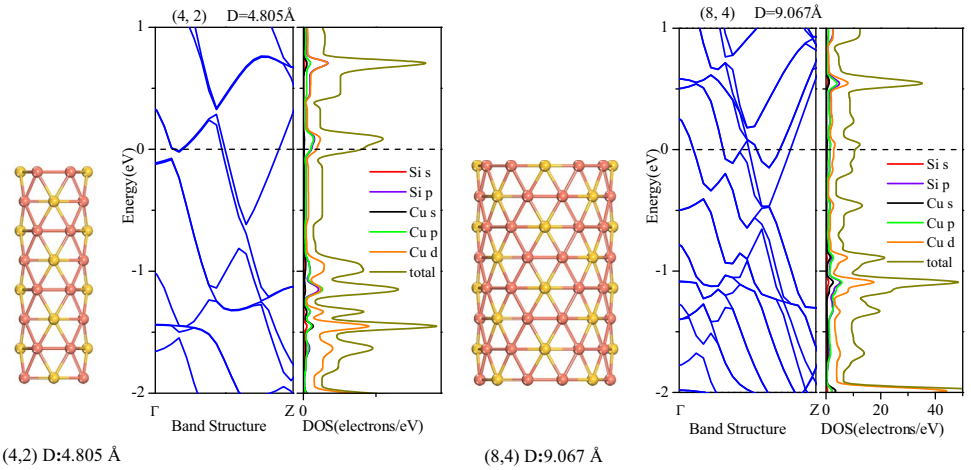


**Fig. 6.** Geometric configuration, band structure and projected density of states (DOS) of the (4, 2), and (8, 4) CuSiNTs. The chiral vector and corresponding diameters (D) are given below the structures.

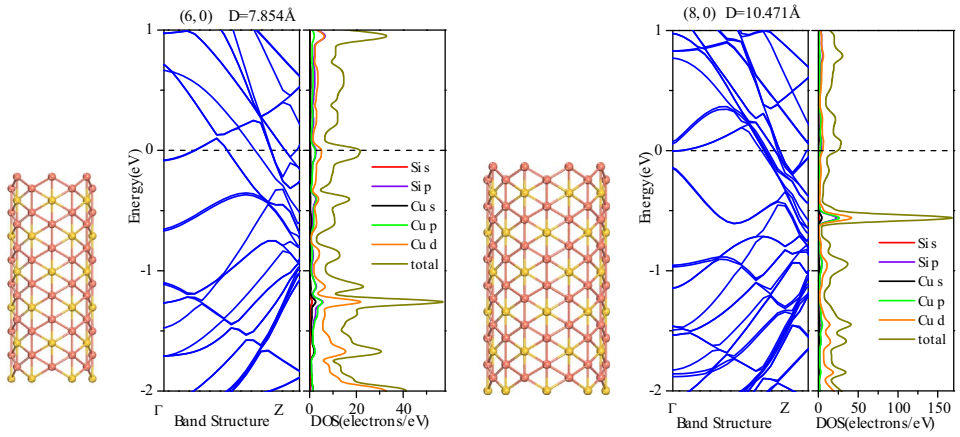


(6,0) D : 7.854 Å (8,0) D : 10.471 Å

**Fig. 7.** Geometric configuration, band structure and density of spin-up and spin-down states (DOS) for the (6, 0), and (8, 0) NT. Band structures for spin-up and spin-down are shown in red and blue.

## Appendix A. Supporting information

Supplementary data associated with this article can be found in the online version at doi:10.1016/j.ssc.2017.01.023.

## References

[1] S. Iijima, Nature 56 (1991) 354.
[2] J. Sha, J. Niu, X. Ma, J. Xu, X. Zhang, Q. Yang, D. Yang, Adv. Mater. 14 (2002) 1219.
[3] S.Y. Jeong, J.Y. Kim, H.D. Yang, B.N. Yoon, S.H. Choi, H.K. Kang, C.W. Yang, Y.H. Lee, Adv. Mater. 15 (2003) 1172.
[4] H.B. Chen, J.D. Lin, J. Yi, Y. Cai, G. Wei, Y.Z. Lin, D.W. Liao, Chin. Chem. Lett. 12 (2001) 1139.
[5] Y.H. Tang, L.Z. Pei, Y.W. Chen, C. Guo, Phys. Rev. Lett. 95 (2005) 116102.
[6] Y.W. Chen, Y.H. Tang, L.Z. Pei, C. Guo, Adv. Mater. 17 (2005) 564.
[7] M. Xie, J. Wang, C.H. Lee, Y.K. Yap, Mater. Res. Soc. Symp. Proc. 1057 (2008) II13.
[8] M. Ara, K. Tomita, H. Tada, Chem. Phys. Lett. 627 (2015) 87.
[9] S.B. Fagan, R.J. Baierle, R. Mota, A.J.R. da Silva, A. Fazzio, Phys. Rev. B 61 (2000) 9994.
[10] S.B. Fagan, R. Mota, R.J. Baierle, G. Paiva, A.J.R. da Silva, A. Fazzio, J. Mol. Struc.-THEOCHEM 539 (2001) 101.
[11] M. Zhang, Y.H. Kan, Q.J. Zang, Z.M. Su, R.S. Wang, Chem. Phys. Lett. 379 (2003) 81.
[12] A.S. Barnard, S.P. Russo, J. Phys. Chem. B 107 (2003) 7577.
[13] B.H. Yan, G. Zhou, J. Wu, W.H. Duan, B.L. Gu, Phys. Rev. B 73 (2006) 155432.
[14] G. Seifert, Th Köhler, H.M. Urbassek, E. Hernández, Th Frauenheim, Phys. Rev. B 63 (2005) 193409.
[15] O. Ponomarenko, M.W. Radny, P.V. Smith, Surf. Sci. 562 (2004) 257.
[16] A.K. Singh, V. Kumar, T.M. Briere, Y. Kawazoe, Nano Lett. 2 (2002) 1243.
[17] A.N. Andriotis, G. Mpourmpakis, G.E. Froudakis, M. Menon, New J. Phys. 4 (2002) 78.
[18] G. Mpourmpakis, G.E. Froudakis, A.N. Andriotis, M. Menon, J. Chem. Phys. 119 (2003) 7498.
[19] A.K. Singh, T.M. Briere, V. Kumar, Y. Kawazoe, Phys. Rev. Lett. 91 (2003) 146802.
[20] C.H. Zhang, J. Shen, Chem. Phys. Lett. 478 (2009) 61.
[21] J. Li, J. Wang, H.Y. Zhao, Y. Liu, J. Phys. Chem. C 117 (2013) 10764.
[22] E. Durgun, S. Tongay, S. Ciraci, Phys. Rev. B 72 (2005) 075420.
[23] L.M. Yang, V. Bačić, I.A. Popov, A.I. Boldyrev, T. Heine, T. Frauenheim, E. Ganz, J. Am. Chem. Soc. 137 (2015) 2757.
[24] B. Delley, Phys. Rev. B 113 (2000) 7756.
[25] J.P. Perdew, K. Burke, M. Ernzerhof, Phys. Rev. Lett. 77 (1996) 3865.
[26] B. Delley, J. Chem. Phys. 92 (1990) 508.
[27] B. Delley, Phys. Rev. B 66 (2002) 155125.
[28] A. Tkatchenko, M. Scheffler, Phys. Rev. Lett. 102 (2009) 073005.
[29] J. Wang, Y. Liu, Y.C. Li, ChemPhysChem 10 (2009) 3119.
[30] J. Wang, H.Y. Zhao, Y. Liu, ChemPhysChem 15 (2014) 3453.